

Performance of the GSN station DGAR-II, 2004–2009

A report in a series documenting the status of the Global Seismographic Network

WQC Report 2010:5
January 25, 2010

Göran Ekström and Meredith Nettles

Waveform Quality Center
Lamont-Doherty Earth Observatory of Columbia University, New York

1 Station performance report: DGAR

This report summarizes a number of observations that are relevant for assessing the past and current quality of the data recorded at one of the stations of the Global Seismographic Network. The purpose of the report is, in part, to document specific problems observed with the data. Some of these problems are related to errors in the available descriptions of station parameters: orientation of the sensors, response functions, polarities. In principle, such errors in the station metadata can be corrected by providing updated station parameters. In practice, this may be difficult in some cases due to lack of knowledge of, or inability to determine, the correct parameters. Other problems are caused by the malfunctioning of some instrument component. Regardless of the cause, it is necessary to document and publicize the lack of accurate and reliable station characteristics, especially when it is not obvious from simple inspection of the data that a problem exists. It is also of value to document the characteristics of stations performing well, both to establish their high quality and to help identify installation and operation procedures that should be emulated at other stations.

1.1 Station DGAR

The station DGAR (Diego Garcia) is located in the Chagos archipelago in the central Indian Ocean (see Figure 1). It is in an excellent location to provide global coverage in earthquake and Earth structure studies. Located approximately 3000 km to the southeast of the rupture zone of the 2004 $M_W=9.3$ Sumatra earthquake, it provided unique and valuable observations for investigations of the mainshock, and for characterization of the still-active aftershock sequence.

The closest GSN station is PALK-II (Pallekele) on the island of Sri Lanka, approximately 1900 km to the northeast of DGAR.

DGAR is part of the IDA (II) component of the IRIS/USGS Global Seismographic Network and is operated by the IDA group at the University of California, San Diego.

1.2 The data

Digital seismic data from DGAR are available from the IRIS DMC beginning in 2004. Here, we consider broadband instruments at the station. The installation in 2004 consisted of a set of STS-1 seismometers and an auxiliary STS-2 sensor. Data from DGAR are included in our standard CMT analysis (Dziewonski et al., 1981; Ekström et al., 2005), and waveform data, travel-time observations, and dispersion curves derived from DGAR data have been used in the development of global and regional tomographic models since the station was installed.

In the analyses described here, we have made use of data collected from the IRIS DMC. We requested and downloaded all long-period (LH) and very-long-period (VH) data available at the DMC for both sensors from the start of operation (2004) until August 2009. We used the currently available station metadata prepared by the IDA group in San Diego (downloaded in December 2009) and also available at the IRIS DMC. Overall, the station has been operated with few data outages since 2004.

1.3 The metadata

The dataless SEED volume for DGAR documents 4 response epochs for the STS-1 (primary) and STS-2 (secondary) sensors at DGAR. The STS-1 1 sps LH channels have location code 00 and we refer to these channels as LHZ-00, LHN-00, and LHE-00. The STS-2 sensor has location code 10 and we refer to the 1 sps channels as LHZ-10, LHN-10, and LHE-10. Epoch boundaries are given at 2004.022 (first data), 2007.115, and 2008.053. The metadata indicate gain and frequency-response changes for the STS-1 at each epoch boundary.

1.4 Scaling analysis

One method for assessing the quality of the data is the systematic comparison of recorded long-period waveforms with synthetic seismograms calculated for known seismic events. This analysis follows the steps described by Ekström et al. (2006). Seismic data for the LH and VH channels from both the STS-1 and STS-2 sensors are collected. Corresponding synthetic waveforms for all earthquakes in the Global CMT catalog (Dziewonski et al., 1981; Ekström et al., 2005) with $M_W \geq 6.5$ are calculated. Correlation coefficients and optimal scaling factors between observed and synthetic waveforms are calculated for the three types of data used in the standard CMT analysis: body waves (B), with periods in the range 50–150 sec, mantle waves (M), with periods in the range 125–350 sec, and surface waves (S), with periods in the range 50–150 sec. Body- and mantle-wave results are discussed here. The scaling factor is only calculated for waveforms with a correlation of 0.75 or greater. The scaling factor is the number by which the synthetic seismogram should be multiplied to maximize the agreement with the observed seismogram. Annual median values of the scaling factors are calculated when four or more individual event scaling estimates are available for the year. Reversed components can be identified by their large negative correlations.

Figure 2 shows the results of our systematic comparison of DGAR waveforms with synthetic seismograms. From the start of operation in 2004 until the present, both the STS-1 and STS-2 signals for large earthquakes correlate well with synthetic waveforms and appear to agree in amplitude. However, only on the vertical component are the background noise levels low enough at long periods (mantle waves) to generate a sufficient number of scaling measurements to calculate an annual median value.

1.5 Noise analysis

A second method for investigating the overall performance of the sensors is to monitor background noise levels for all seismic channels, after conversion of the data to ground acceleration. We calculate hourly rms

values of the time-domain seismic signal in narrow frequency bands, and convert the rms values to a power spectral density (PSD) at that frequency using Parseval’s theorem. For each month, we then calculate the low-noise value at each frequency by determining the PSD amplitude not exceeded 10% of the time.

The PSD data provide much information about the station and the sensors. Figure 3 shows the monthly low-noise estimate for each LH channel at 72-s period since 1990. The first observation is that the station has been providing data without major outages since 2004. Only in 2007 and in early 2008 are there gaps of a few months. Second, the noise data reflect that DGAR is a naturally very noisy site, and that the noise characteristics have remained stable since 2004.

The STS-2 noise levels are similar to those of the STS-1 at 72-s period. For most months, the vertical noise on the STS-1 is lower than on the STS-2; the opposite is true for the horizontal components.

1.6 Inter-sensor coherence

An additional method for assessing the quality and calibration of the recorded signals is to calculate inter-sensor coherence. This analysis is possible when more than one sensor is operated in the same location. At DGAR, this is possible for the entire period of operation, 2004–2009, during which time both STS-1 and STS-2 instruments have been operating.

We calculate the coherence of the deconvolved vertical, N–S, and E–W components. In our standard analysis, the coherence is calculated for ~ 2 -hour-long time windows containing signals for earthquakes with $M_W \geq 6.5$ (the same events used in the scaling analysis). For DGAR, we also perform a second coherence analysis, based on continuous data. This analysis is pursued because (1) background noise levels are so high at DGAR that they interfere with long-period earthquake signals even from large earthquakes, and (2) background ground noise is so large that it dominates other instrument-specific noise sources, thus generating a dominant, nearly continuous, common input signal for the two instruments. In the analysis of continuous data, we use 4-hour-long time windows for the coherence analysis.

For each pair of seismograms (earthquake or continuous), we calculate the coherence in narrow frequency bands around 32 s, 64 s, 128 s and 256 s. If the coherence is greater than 0.95, the value is stored together with the complex scaling factor (represented here as a scaling factor and phase shift) that should be applied to the secondary-sensor data to bring the two time series into the best agreement. In the following, the discussion is based on the assumption that the secondary (STS-2) sensor is properly calibrated and that deviations from a scaling factor of 1.0 and a phase shift of 0° should be attributed to differences between the true and reported response functions of the primary (STS-1) sensor.

Figure 4 shows the results of the coherence analysis for the vertical component. The measurements are very consistent and stable, with a scaling factor close to 0.95 for all periods, and a phase shift very close to 0° . The $\sim 5\%$ deviation from 1.0 suggests that the true gain of the STS-1 may be less than that stated in the metadata by this amount.

Figure 5 shows the amplitude and phase differences for the N–S components. The relatively small number of measurements in the top panels (based on earthquake signals) is a result of the high-amplitude background noise. A number of 256-s measurements in 2005 stand out as anomalous, suggestive of a temporary response problem. The coherence analysis based on the continuous data provides a larger number of measurements (bottom panels), and it becomes clear that the N–S component went through a gradual loss of long-period gain in early 2005, and then a slow recovery. A frequency-independent difference of $\sim 5\%$ between the STS-1 and STS-2 is also apparent.

Figure 6 shows the results for the E–W components, which show a similar pattern to the N–S components, except that the transient loss of long-period gain in 2005 is much smaller, a few per cent.

1.7 Polarization analysis

The orientation of the horizontal components can be assessed empirically by comparing observed and synthetic waveforms, and finding the angle by which the horizontal components should be rotated in order to maximize the agreement. We follow the approach described by Ekström and Busby (2008) for such a comparison, using the observed and synthetic waveforms from Global CMT analysis.

We apply the method of Ekström and Busby (2008) to the same dataset used in the scaling analysis. Figure 7 shows the individual measurements for the period of operation of the different channels. Overall, the number of useful observations in the surface-wave band is quite large, considering the very high level of horizontal noise at DGAR. The median rotation angles for the STS-1 and the STS-2 sensors are both 1° , and the spreads of observations are small. The median estimates for the entire period of operation are given in Table 1.

Comp. 1	Comp. 2	First	Last	# Obs.	N	Az 1	Az 2	25%	Med.	75%
LHE-00	LHN-00	20040205	20090830	231	47	90	0	-1	1	3
LHE-10	LHN-10	20040128	20090830	233	54	90	0	-1	1	3

Table 1: Statistics of sensor-rotation angles estimated in this study. Columns are the channel names, the dates of the first and last observations considered in making the estimate, the total number of observations, the number of observations of acceptable quality, the reported azimuths of sensitivity of the two channels, the median polarization-angle deviation from the reported orientation together with the range of the second (25%) and third (75%) quartiles of the observations.

1.8 Example seismograms

The anomalies described here agree with observations we have made in our routine analysis of waveforms for the determination of CMT earthquake parameters. When confronted with the seismograms for an individual earthquake, it is often difficult to assess whether a poor fit is due to incorrect source parameters, inadequate modeling of wave propagation through an Earth model, or some problem with the recorded seismograms. Here, we have included some examples of data that illustrate the characteristics of the types of problems that we have encountered with data from the DGAR station.

Figure 8 shows an example of three-component mantle-wave data for the March 28, 2005, $M_W=8.6$ southern Sumatra earthquake. This earthquake occurred during the period of anomalous response on the N-S component (Figure 5). It is not immediately evident from the waveforms, or the fit of the synthetics, that there is anything wrong with the data. However, when comparing the optimal scaling coefficient for the STS-1 and STS-2 seismograms, a 20% difference is observed in the mantle-wave period band (150–400 s).

The top panel of Figure 9 shows a comparison between surface-wave seismograms recorded on the STS-1 seismometer and the corresponding synthetic waveforms for an event on June 23, 2009. The waveforms are nicely matched. The bottom panel of Figure 9 shows the comparison between seismograms recorded on the STS-2 seismometer and the corresponding synthetic waveforms for the same event. The fits are also good for all components of this sensor. The only clear difference between the STS-1 and STS-2 seismograms is an amplitude difference of $\sim 5\%$ between the two sensors.

2 Summary and analysis

At the time of writing (January, 2010), the GSN station DGAR is performing well. Noise levels on islands such as Diego Garcia are unavoidably high. Our analysis suggests that the station has been producing high-quality data for most of the period since installation (2004), and that the STS-2 provides high-quality backup data streams.

The coherence analysis shows that the N–S STS-1 sensor went through a year-long transient perturbation to its long-period response in 2005. This is best documented in measurements derived from continuous data (Figure 5). The character of this transient is similar to those documented for other stations equipped with STS-1 sensors (Ekström et al., 2006, Ekström and Nettles, WQC Report 2010:2), but is unusual in its small amplitude and in that a recovery to the stated response occurred over several months, potentially without intervention. The E–W component displays a much smaller anomaly, which appears to coincide temporally with the transient on the N–S component.

A difference in the frequency-independent gain of the STS-1 and STS-2 sensors of $\sim 5\%$ is apparent from the coherence analysis.

3 Conclusions and recommendations

This analysis shows that DGAR currently is generating data of high quality. While more detailed analysis would be required to establish that the relative response characteristics are accurate to within the 1% tolerance of the original GSN design goals (IRIS, 1985; Lay et al., 2002), our assessment is that DGAR generates GSN quality data, at least at long periods.

The relative and absolute calibrations of the STS-1 and STS-2 sensors are uncertain, since our analysis indicates a difference of $\sim 5\%$ between the two responses.

Our coherence analysis indicates that the horizontal STS-1 seismometers suffered transient long-period gain loss similar in character to that documented at several other stations equipped with STS-1 seismometers (Ekström et al., 2006). To the extent that it is possible to identify any environmental factors that can be correlated with the occurrence of the problem, or its disappearance, this may help in the investigation of other stations that may exhibit the same behavior. We note also that the transient character of this problem at DGAR provides additional arguments for the regular recording of diagnostic calibration pulses. Simple step calibrations would be sufficient for this purpose (e.g., Ekström and Nettles, 1997).

4 References

- Dziewonski, A. M., T.-A. Chou, and J. H. Woodhouse, Determination of earthquake source parameters from waveform data for studies of global and regional seismicity, *J. Geophys. Res.*, 86, 2825–2853, 1981.
- Ekström, G., A. M. Dziewonski, N. N. Maternovskaya, and M. Nettles, Global seismicity of 2003: Centroid-moment tensor solutions for 1087 earthquakes, *Phys. Earth Planet. Inter.*, 148, 327–351, 2005.
- Ekström, G., C. A. Dalton, and M. Nettles, Observations of time-dependent errors in long-period gain at global seismic stations, *Seism. Res. Lett.*, 77, 12–22, 2006.
- Ekström, G., and R. W. Busby, Measurements of seismometer orientation at USArray Transportable and Backbone stations, *Seism. Res. Lett.*, 79, 554–561, 2008.
- Ekström, G., and M. Nettles, Calibration of the HGLP seismograph network and centroid-moment tensor analysis of significant earthquakes of 1976, *Phys. Earth Planet. Inter.*, 101, 219–243, 1997.
- Ekström, G., and M. Nettles, Performance of the GSN station KIP-IU, 1988–2009, Waveform Quality Center Report 2010:2, 2010.

- IRIS, *The design goals for a new global seismographic network*, IRIS GSN committee report, 31 pages, 1985.
- Lay, T., J. Berger, R. Buland, R. Butler, G. Ekström, B. Hutt, B. Romanowicz, *Global seismic network design goals update 2002*, IRIS GSN committee report, 2002.
- Peterson, J., Observations and modeling of background seismic noise, *U. S. Geol. Surv. Open-file Rep. 93-322*, 1–45, 1993.

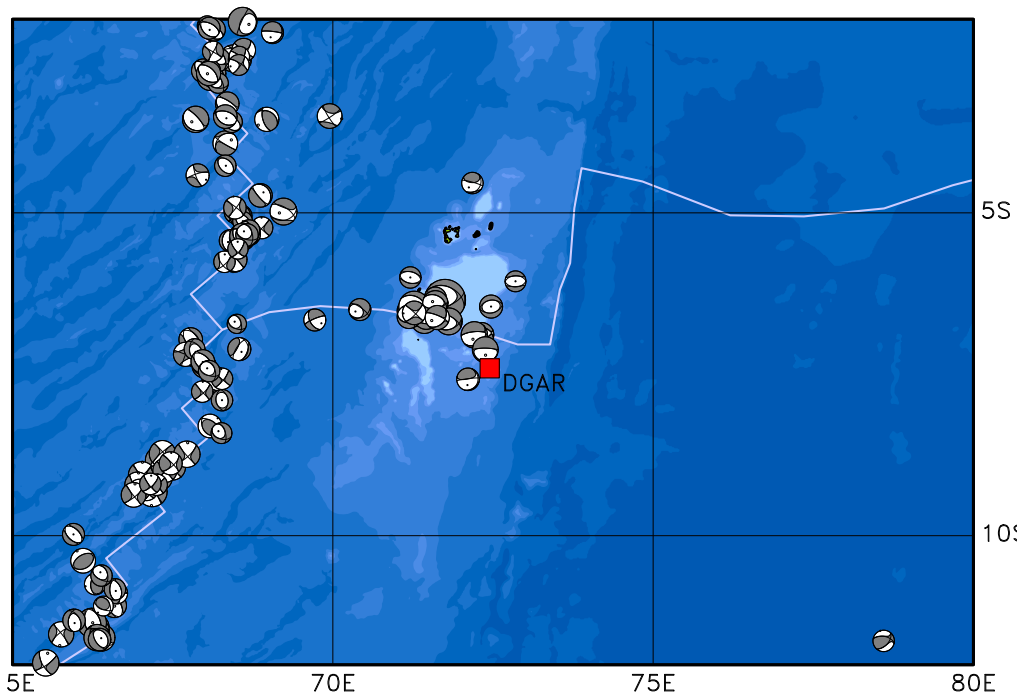


Figure 1: Map showing the location of DGAR (red square) in the Chagos archipelago in the central Indian Ocean. Grey focal mechanisms show the locations and moment tensors of earthquakes in the Global CMT catalog. The closest GSN station is PALK-II, located ~1900 km to the northeast on the island of Sri Lanka.

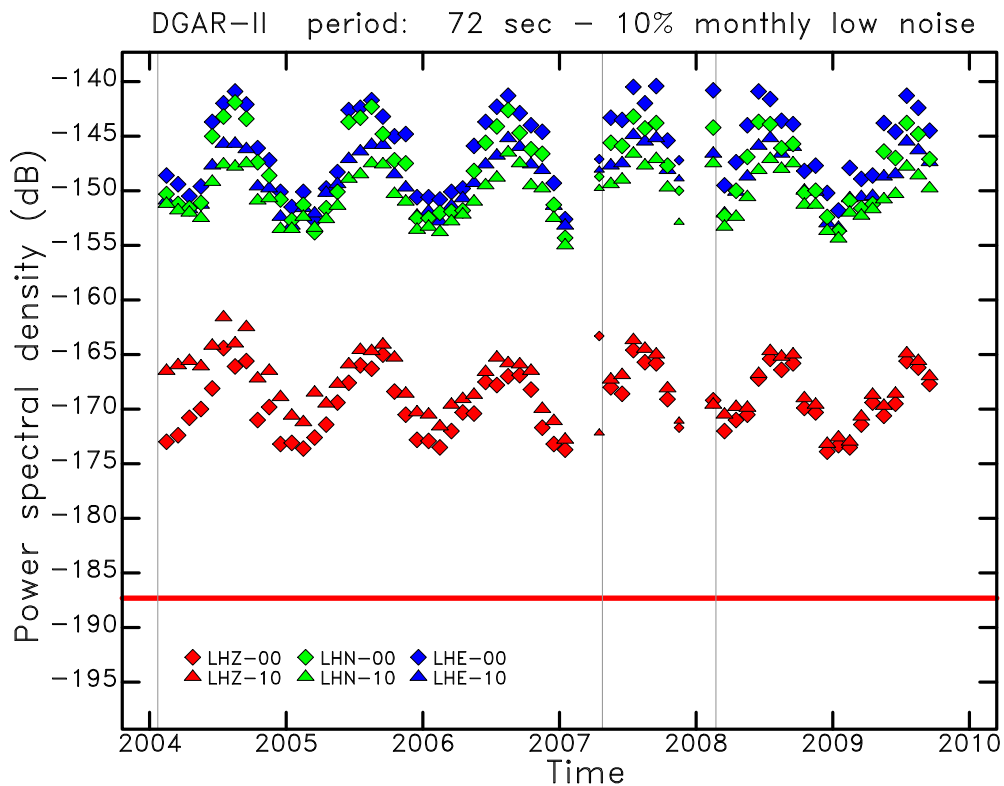


Figure 3: Monthly PSD of ground acceleration at 72-s period for all long-period (LH) channels at DGAR for the period 2004–2009. Smaller symbols are used for months with fewer available hourly measurements. Each component and sensor is represented by a distinct symbol and color. The red horizontal line indicates the level of Peterson’s (1993) Low Noise Model (LNM) at 72 s. The thin vertical lines show the times of epoch boundaries in the station metadata. A clear seasonality is seen in the very high vertical and horizontal noise levels. The horizontal components of the STS-2 have lower noise levels than the STS-1 at this period.



Figure 4: Diagram shows the result of coherence analysis for the vertical components of the STS-1 and STS-2 sensors. Top two panels show results only for time windows corresponding to large earthquakes. Bottom two panels show results derived from continuous data. In top panels, each symbol represents a measurement of coherence for a $M_W \geq 6.5$ earthquake. In bottom panels, each measurement is based on 4 hours of continuous data. The minimum coherence plotted is indicated by c . The scaling and phase shift between the two time series is shown at four different periods. The plots show a deviation of the coherence measurements of $\sim 5\%$ from a scaling of 1.0. The measured phase shift is 0° . The thin vertical lines show the times of epoch boundaries in the station metadata.

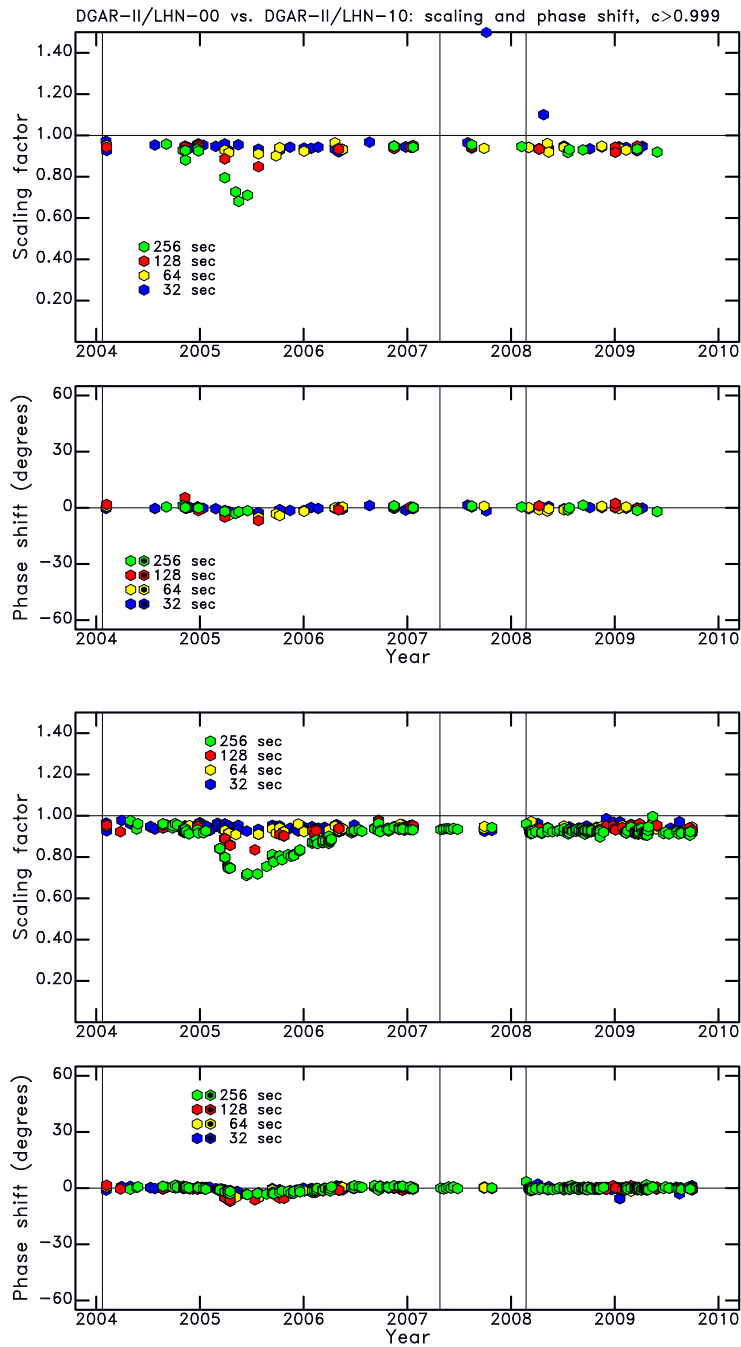


Figure 5: Same as Figure 4, but for the North-South components. Measurements at the longest period show a significant deviation during 2005, consistent with a loss of gain of the STS-1 seismometer, followed by a slow recovery. This is most clearly seen in the analysis of the continuous data (bottom panels). An overall gain difference of $\sim 5\%$ at all times is suggested by the measurements.

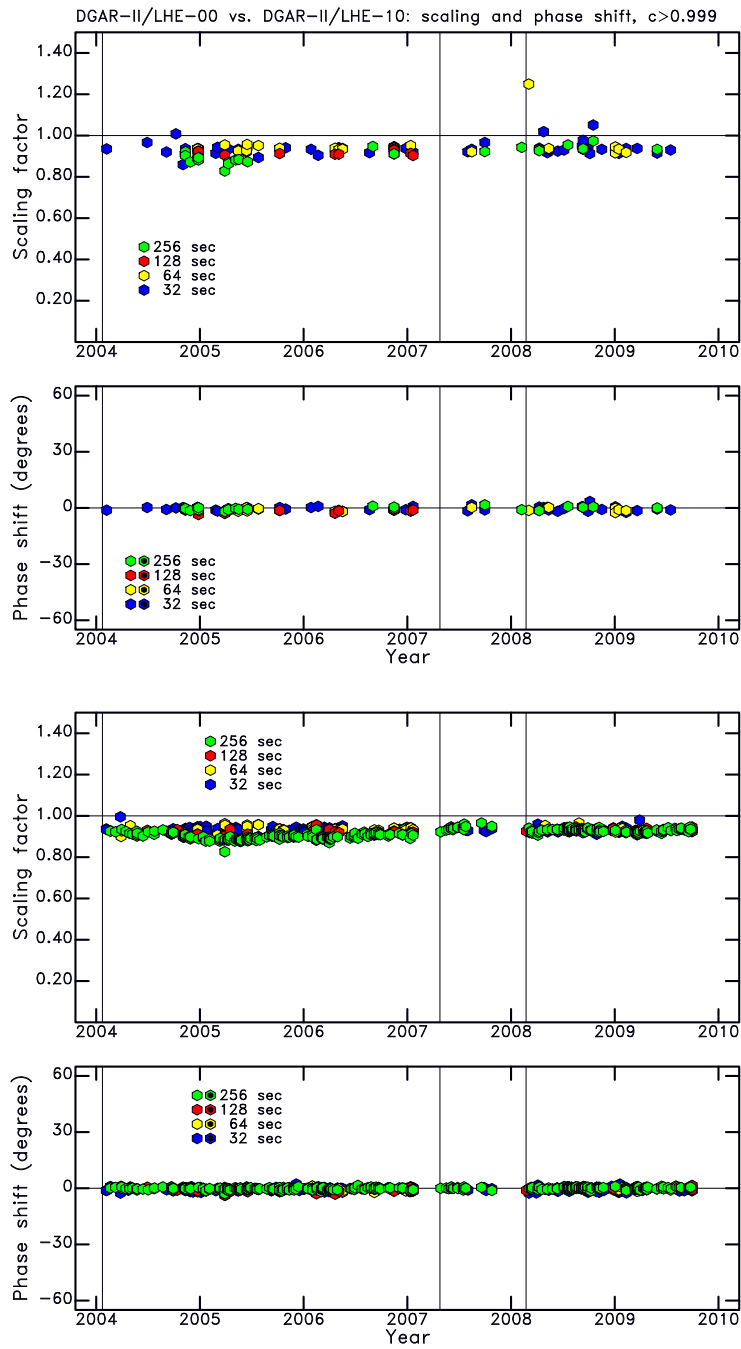


Figure 6: Same as Figure 4, but for the East-West components. A small loss of long-period gain in 2005 is suggested by the data. An overall gain difference of $\sim 5\%$ at all times is suggested by the measurements.

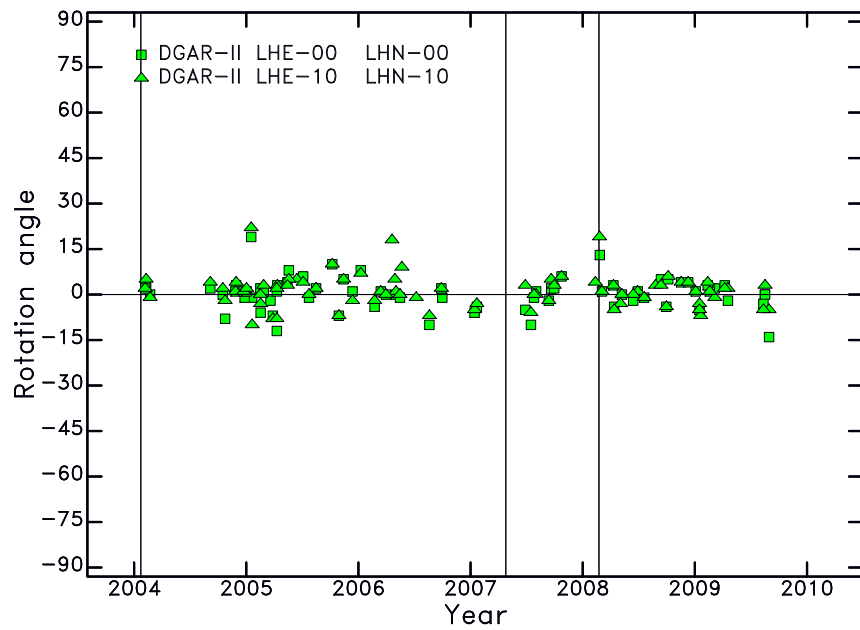


Figure 7: Individual measurements of polarization angle as a function of time. All measurements for the period of operation are shown. Symbols represent measurements obtained in the surface-wave band of the CMT analysis. More than 50% of the observations lie in the range -1° to $+3^\circ$. The thin vertical lines show the times of epoch boundaries in the station metadata.

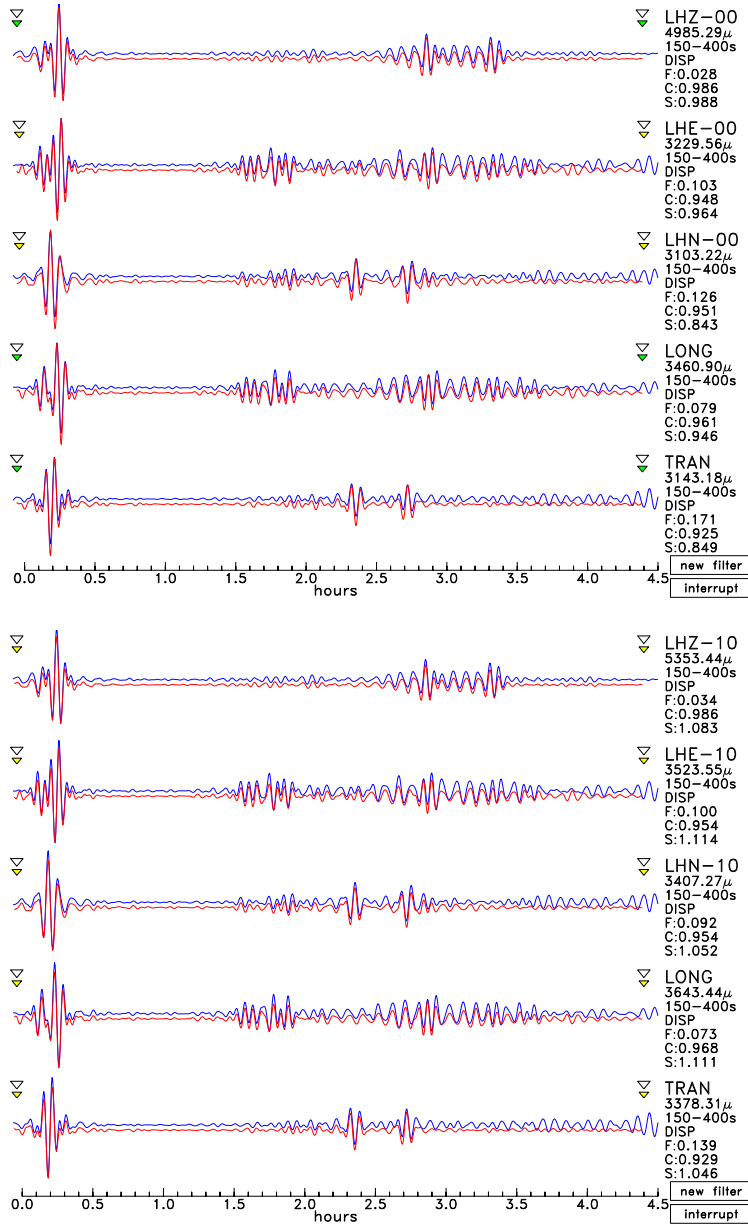


Figure 8: Comparison of observed (blue traces) and synthetic (red traces) mantle-wave seismograms for the March 28, 2005, $M_W=8.6$ southern Sumatra earthquake. The channel name, maximum displacement, and values for the three parameters residual misfit (F), correlation (C) and scaling factor (S) are given to the right of each waveform. (Top) Seismograms for the STS-1 sensor. (Bottom) Seismograms for the STS-2 sensor. The observed STS-1 N-S seismogram is smaller than the STS-2 seismogram by $\sim 20\%$.

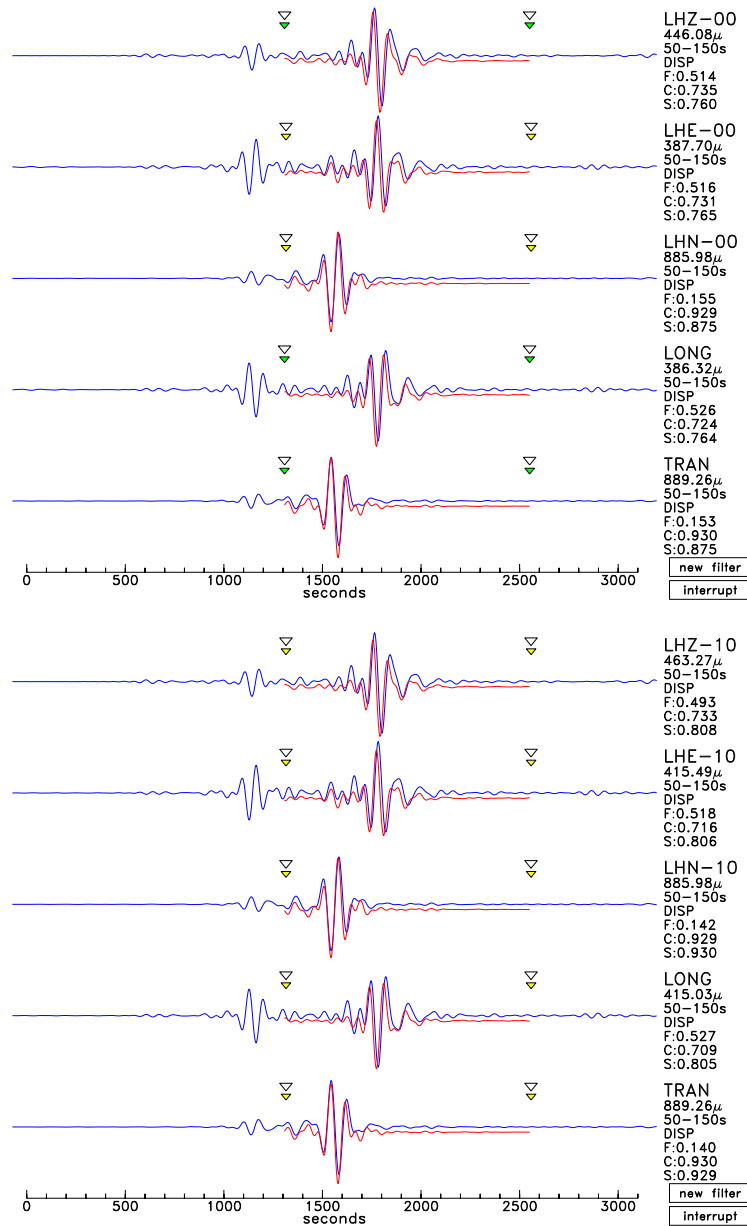


Figure 9: (Top) Observed (STS-1) and synthetic surface-wave seismograms for an $M_W=7.4$ earthquake on January 3, 2009. The fit is good. (Bottom) Observed (STS-2) and synthetic body-wave seismograms for the same earthquake, but recorded on the STS-2 seismometer. The fit to all three components is good. The scaling factors for the STS-2 are bigger than those of the STS-1 by $\sim 5\%$, consistent with a frequency-independent difference in the reported gains.